

# ChemPhysChem

Supporting Information

## **Solving the Puzzle of the Carbonic Acid Vibrational Spectrum – an Anharmonic Story**

Jonas Schlagin, Dennis F. Dinu, Jürgen Bernard, Thomas Loerting, Hinrich Grothe, and Klaus R. Liedl\*

# Supplementary Information for: Solving the puzzle of the carbonic acid vibrational spectrum - An anharmonic story

Jonas Schlagin,<sup>+[a]</sup> Dennis F. Dinu,<sup>[a]</sup> Jürgen Bernard,<sup>[b]</sup> Thomas Lörting,<sup>[b]</sup>  
Hinrich Grothe,<sup>[c]</sup> Klaus R. Liedl<sup>\*[a]</sup>

<sup>[a]</sup> Institute of General, Inorganic and Theoretical Chemistry,  
University of Innsbruck  
Innrain 80-82, 6020 Innsbruck  
Email: Klaus.Liedl@uibk.ac.at

<sup>[b]</sup> Institute of Physical Chemistry,  
University of Innsbruck  
Innrain 52c, 6020 Innsbruck <sup>[c]</sup> Institute of Materials Chemistry,  
TU Wien  
Getreidemarkt 9/165, 1060 Wien

---

With this supplementary information we provide the complete assignment of argon trapped H<sub>2</sub>CO<sub>3</sub> species, the normal mode decomposition of each fundamental and their vibrational analysis as well as a visualisation of said vibrational analysis.

---

## Main contributions of internal coordinates according to the normal mode decomposition

Table S1: Normal mode decomposition of cc-H<sub>2</sub>CO<sub>3</sub>

harm. [cm <sup>-1</sup> ].	chemist Notation	normal mode decomposition <sup>1</sup>
3823	$\nu_{\text{symm. OH}}$	99.92 % OH bond (49.96 each)
3821	$\nu_{\text{anti. OH}}$	99.96 % OH bond (49.98 % each)
1843	$\nu_{\text{symm. C=O}}$	72.68 % C=O bond, 14.82 % C-O bond (7.41 % each)
1485	$\nu_{\text{anti C-O}}$	55.76 % C-O bond (27.88 % each) 29.24 % COH angle (14.62 % each)
1307	$\delta_{\text{ip symm. OH}}$	82.86 % COH angle (41.43 % each), 14.69 % C=O bond
1181	$\delta_{\text{ip anti. OH}}$	54.44 % COH angle (27.22 % each), 43.58 % C-O bond (21.79 % each)
987	$\nu_{\text{symm. C-O}}$	93.74 % C-O bond (46.87 % each), 4.17 % C=O bond
806	$\delta_{\text{oop OCO}}$	98.06 % C out of plane coordinate
606	$\delta_{\text{ip C=O}}$	79.84 % O=CO angle (39.92 % each), 11.22 % COH angle (5.61 % each)
602	$\delta_{\text{oop symm. OH}}$	48.14 % O=COH dihedral, 48.14 % OCOH dihedral
550	$\delta_{\text{ip C-O}}$	55.99 % OCO angle, 26.16 % O=CO angle (13.13 % each)
532	$\delta_{\text{oop anti OH}}$	50.00 % O=COH dihedral, 50.00 % OCOH dihedral

<sup>1</sup> Normal mode decomposition calculated as described in Ref. [1]

Table S2: Normal mode decomposition of *ct*-H<sub>2</sub>CO<sub>3</sub>

harm. [cm <sup>-1</sup> ]	chemist Notation	normal mode decomposition <sup>1</sup>
3822	$\nu$ OH	99.93 % OH bond (87.97 % trans-OH, 11.96 % cis-OH)
3819	$\nu$ OH	99.91 % OH bond (87.92 % cis-OH, 11.99 % trans-OH)
1894	$\nu$ C=O	76.54 % C=O bond, 12.39 % C-O bond (6.43 % trans-CO, 5.96 % cis-CO)
1426	$\nu$ C-O	57.85 % C-O bond (33.71 % cis-CO, 24.15 % trans-CO), 20.66 % cis-COH angle
1289	$\delta_{ip.}$ OH	84.88 % COH angle (47.04 % cis-COH, 37.84 % trans-COH)
1178	$\delta_{ip.}$ OH	55.05 % COH angle (34.01 % trans-COH, 21.04 % cis-COH), 32.77 % trans-CO bond
974	$\nu$ C-O	89.71 % C-O bond (54.34 % cis-CO, 35.37 % trans-CO)
793	$\delta_{oop.}$ OCO	95.44 % C out of plane coordinate
610	$\delta_{ip.}$ C=O	79.86 % O=CO angle (42.46 % trans-O=CO, 37.40 % cis-O=CO)
569	$\delta_{ip}$ C-O	55.61 % OCO angle, 25.33 % O=CO angle (14.71 % trans-O=CO, 10.62 % cis-O=CO)
551	$\delta_{oop.}$ OH	79.45 % O=COH dihedral, 18.08 % OCOH dihedral
488	$\delta_{oop.}$ OH	18.08 % O=COH dihedral, % 81.90 OCOH dihedral

<sup>1</sup> Normal mode decomposition calculated as described in Ref. [1]

Table S3: Normal mode decomposition of *cc*-D<sub>2</sub>CO<sub>3</sub>

harm. [cm <sup>-1</sup> ]	chemist notation	normal mode decomposition <sup>1</sup>
2784	$\nu_{symm.}$ OD	99.90 % OD bond (49.95 % each)
2778	$\nu_{anti.}$ OD	99.96 % OD bond (49.98 % each)
1830	$\nu_{symm.}$ C=O	73.06 % C=O bond, 15.02 % C-O bond (7.51 % each)
1415	$\nu_{anti.}$ C-O	64.26 % C-O bond (32.13 % each), 20.54 % COH angle (10.27 % each)
1092	$\delta_{ip}$ <i>symm.</i> OD	81.20 % COD angle (40.60 % each), 15.17 % C=O bond
975	$\delta_{ip}$ <i>anti.</i> OD	62.90 % COD angle (31.45 % each), 36.12 % C-O bond (18.06 % each)
899	$\nu_{symm.}$ C-O	91.78 % C-O bond (45.89 % each)
804	$\delta_{oop}$ OCO	86.56 % C out of plane coordinate, 12.74 % O=COD dihedral
559	$\delta_{ip}$ C=O	78.68 % O=CO angle (39.34 % each), 9.26 % C-O bond (4.63 % each)
508	$\delta_{oop}$ <i>symm.</i> OD	52.26 % O=COD dihedral, 42.98 % OCOD dihedral
434	$\delta_{ip}$ C-O	55.74 % OCO angle, 26.72 % O=CO (13.36 % each)
404	$\delta_{oop}$ <i>anti.</i> OD	57.40 % O=COD dihedral, 42.60 % OCOD dihedral

<sup>1</sup> Normal mode decomposition calculated as described in Ref. [1]

Table S4: Normal mode decomposition of *ct*-D<sub>2</sub>CO<sub>3</sub>

harm [cm <sup>-1</sup> ]	chemist notation	normal mode decomposition <sup>1</sup>
2782	$\nu$ OD	99.94 % OD bond (86.38 % cis-OD, 13.56 % trans-OD)
2779	$\nu$ OD	99.91 % OD bond (86.32 % trans-OD, 13.59 % cis-OD)
1879	$\nu$ C=O	76.54 % C=O bond, 12.39 % C-O bond (6.43 % cis-CO, 5.96 % trans-CO)
1356	$\nu$ C-O	57.85 % C-O bond (33.71 % trans-CO, 24.14 cis-CO), 29.9 % COD angle (20.67 % trans-COD, 9.23 % cis-COD)
1059	$\delta_{\text{ip.}}$ OD	84.88 % COD angle (47.06 trans-COD, 37.82 cis-COD)
971	$\delta_{\text{ip.}}$ OD	55.07 % COD angle (34.07 % cis-COD, 21.00 % trans-COD), 42.40 % C-O bond (32.75 % cis-CO, 9.65 % trans-CO)
899	$\nu$ C-O	89.71 % C-O bond (54.31 % trans-CO, 35.4 cis-CO)
792	$\delta_{\text{oop.}}$ OCO	86.01 % C out of plane coordinate
581	$\delta_{\text{ip.}}$ C=O	79.85 % O=CO angle (42.33 % trans-O=CO, 37.52 % cis-O=CO)
497	$\delta_{\text{oop.}}$ OD	55.66 % OCO angle, 25.32 % O=CO angle (14.58 cis-O=CO, 10.74 % trans-O=CO)
423	$\delta_{\text{ip.}}$ C-O	83.66 % O=COD dihedral
358	$\delta_{\text{oop.}}$ OD	75.21 % OCOD dihedral, 23.63 % O=COD dihedral

<sup>1</sup> Normal mode decomposition calculated as described in Ref. [1]

## Potential energy surface benchmark

We calculated both a frozen-core (CCSD(T)-F12/cc-pVTZ-F12) and a core-correlation (CCSD(T)-F12/cc-cpVTZ-F12) PES with up to 3-mode coupling. In the subsequent VCI calculations, the core-correlation PES systematically yields higher frequencies (roughly 0.25 %) than the frozen-core PES (cf. Table S5). This does not significantly improve our assignment. A comparable shift is to be expected for both conformers. Core correlation causes a significant computational overhead. As we aim for a PES with up to 4-mode coupling, we decided to continue our study with the frozen-core PES.

Table S5: VCI results for two different potential energy surfaces with up to 3-mode couplings, using CCSD(T)-F12/VTZ-F12 (frozen core) and CCSD(T)-F12/CVTZ-F12 (core correlation).

Mode	frozen core			core correlation			relative deviation / %		
	Harm	VSCF	VCI	Harm	VSCF	VCI	Harm	VSCF	VCI
12 ( A1 )	3823.35	3637.18	3594.58	3827.98	3643.09	3602.62	0.12	0.16	0.22
11 ( B1 )	3820.78	3608.4	3588.7	3825.32	3615.69	3596	0.12	0.20	0.20
10 ( A1 )	1843.23	1813.33	1801.74	1846.4	1817.74	1806.33	0.17	0.24	0.25
9 ( B1 )	1484.7	1451.45	1420.03	1487.48	1455.53	1422.79	0.19	0.28	0.19
8 ( A1 )	1306.65	1292.87	1245.94	1306.64	1295.45	1248.97	0.00	0.20	0.24
7 ( B1 )	1180.55	1176.05	1127.98	1181.49	1178.34	1129.27	0.08	0.19	0.11
6 ( A1 )	987.38	973.98	964.6	990.11	977.64	968.11	0.28	0.38	0.36
5 ( B2 )	805.97	801.03	791.82	809.17	805.32	795.95	0.40	0.54	0.52
4 ( B1 )	605.92	605.85	596.19	608.33	609.22	599.33	0.40	0.56	0.53
3 ( B2 )	602.35	698.49	613.78	602.85	698.61	614.48	0.08	0.02	0.11
2 ( A1 )	549.96	556.61	539.13	552.22	559.83	542.1	0.41	0.58	0.55
1 ( A2 )	531.66	648.92	557.56	532.19	644.15	554.39	0.10	-0.74	-0.57

## Assignment of individual spectral windows for cc-H<sub>2</sub>CO<sub>3</sub>, ct-H<sub>2</sub>CO<sub>3</sub> and cc-D<sub>2</sub>CO<sub>3</sub>

### Resonance analysis and resonating bands

Due to the way how vibrational states are obtained within the VCI approach, by selecting different sets of configurations of the VSCF wavefunctions, one obtains different VCI states with similar contributions of configurations. Thus, in some cases, it is not directly obvious, which VCI calculated vibrational state represents the vibration of interest indicating whether it is a fundamental, overtone, or combination band. In *Molpro*, there are two different ways how to choose the VCI state that represents the vibration of interest:

- One can choose a VCI state based on the coefficients of the configurations that contribute to that VCI state. The configuration with the highest leading coefficient determines the identity of the VCI state. For example, if one is interested in a specific fundamental vibration, the configuration that includes the normal mode representing this fundamental and has the highest leading coefficient gets picked. Usually, if the magnitude of the highest leading coefficient is above 0.8, the VCI state identity is designated as unambiguous. Otherwise, a unique state identity is not possible and one has to consider a resonance analysis.
- One can calculate the overlap integral between the VCI state and the corresponding harmonic state and the state with the highest overlap value gets picked. Similar to the above case, the state identity is only unambiguous if only one harmonic

overlap has a considerable magnitude.

In the following, we rely on the leading coefficients as the selection metric. Since it is longer implemented and the successful assignment of this method is well documented through various works.<sup>[2-9]</sup> Calculating the overlap integral is a valid choice as well and yields the same qualitative statement, in most cases.

### **Non-deuterated argon experiment**

From earlier thermodynamic considerations, the two stable conformers, *cc*-H<sub>2</sub>CO<sub>3</sub> and *ct*-H<sub>2</sub>CO<sub>3</sub>, likely occur in the spectrum. The experimental Gibbs free energy difference between these conformers is only  $\Delta G = 4 \text{ kJ mol}^{-1}$  at 210 K.<sup>[10]</sup> In the experiment, carbonic acid was directly sublimated into the cryostat for isolation in the matrix. We assume that both conformers are isolated during that process and, hence, consider both conformers in the assignment.

### **The OH-stretching region of carbonic acid**

The first region of interest that appears in the spectrum is the OH stretching region. From the normal mode decomposition (see Tables S1 and S2) one can see that the notation of this region as the OH stretching region is justified. This is because almost 100 % of the internal coordinate contribution is made up of a change in the OH bondlength. It is the hardest spectral window to assign due to the very high overlap of bands that arise from water and carbon dioxide contaminations.

### **Contamination in the experimental data from J. Bernard**

In Figure S1 bands due to water contamination according to Refs.<sup>[9,11]</sup> and carbon dioxide according to Ref.<sup>[9]</sup> are assigned accordingly. This contamination is expected due to the favorable decomposition of carbonic acid in non-water-free environments.<sup>[12]</sup> The contamination causes an arising of additional bands, of which especially the OH stretch vibrations of water are problematic in the particular region we are investigating here. Also, water is known to rotate in noble gas matrices.<sup>[11]</sup> Therefore, not only bands that arise from the vibration appear in the spectrum, but also the rotational-vibrational bands.<sup>[9,11]</sup> All of this makes this spectral window the most difficult to assign. Therefore, to obtain a correct assignment, one must rule out all bands that can be assigned to contaminations (H<sub>2</sub>O, CO<sub>2</sub>) and work with the remaining peaks.

With the knowledge of which peaks appear due to water and carbon dioxide, we can move on to the peaks that may be assigned to specific carbonic acid vibrations.

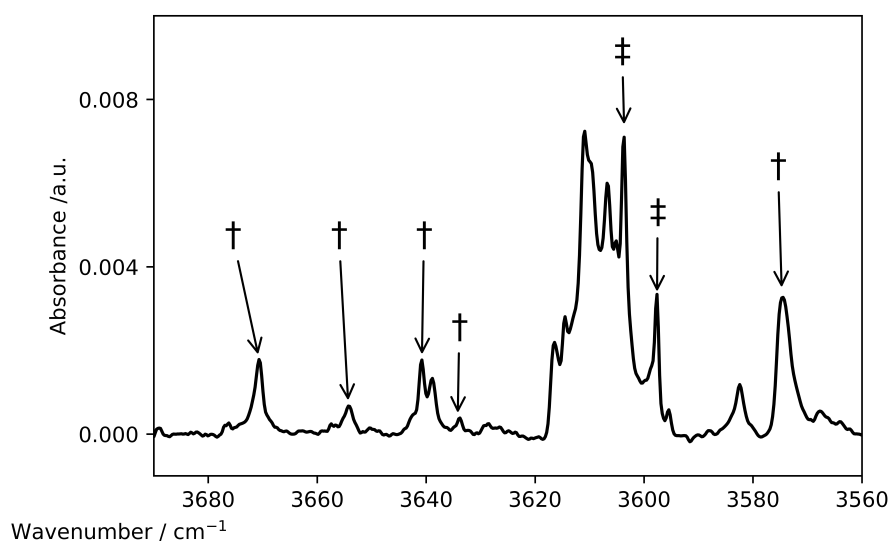


Figure S1: OH stretching region of the carbonic acid spectrum in argon matrix. Water contaminations in the OH-stretching region are marked as daggers †, Carbon dioxide contaminations are marked as double daggers ‡.

### Other spectral windows that can be assigned to H<sub>2</sub>CO<sub>3</sub>

For the assignment of newly assigned bands we refer to the main part of this publication. For the assignment of all previously known vibrational bands we refer to the original work of Jürgen Bernard<sup>[10,13]</sup>

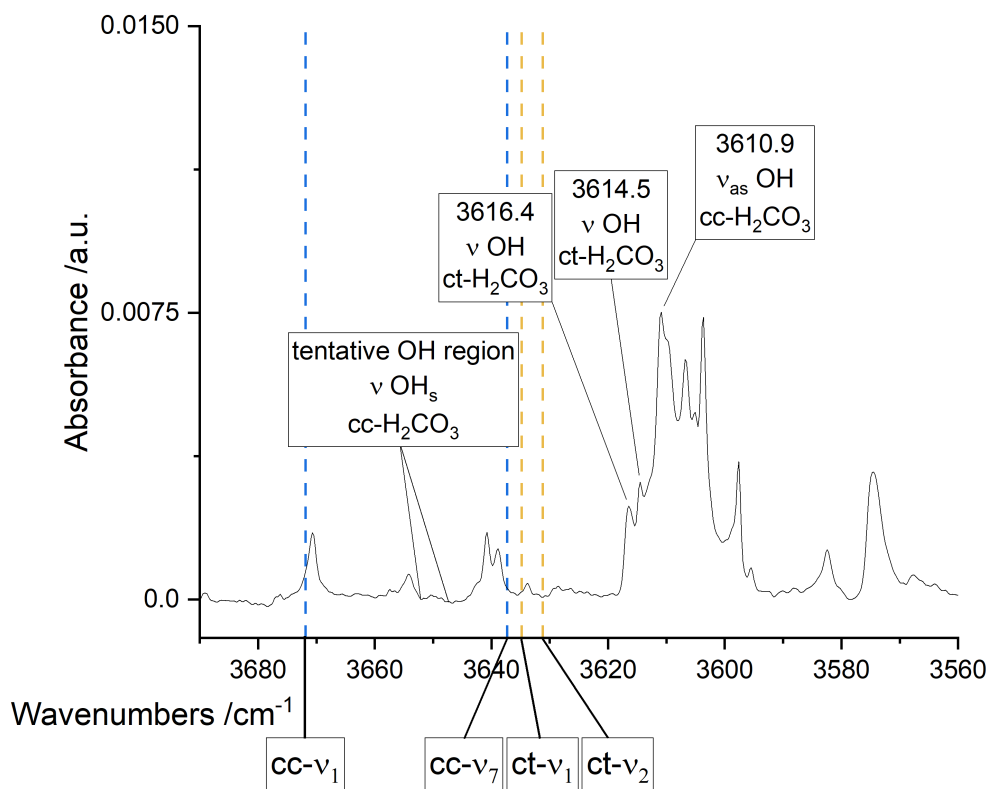


Figure S2: Assignment of the OH stretching region of the H<sub>2</sub>CO<sub>3</sub> spectrum. VCI calculated wavenumbers are plotted in dashed lines (blue = cc-conformer; yellow = ct-conformer). Bands not assigned are due to H<sub>2</sub>O and CO<sub>2</sub>, see Figure 4

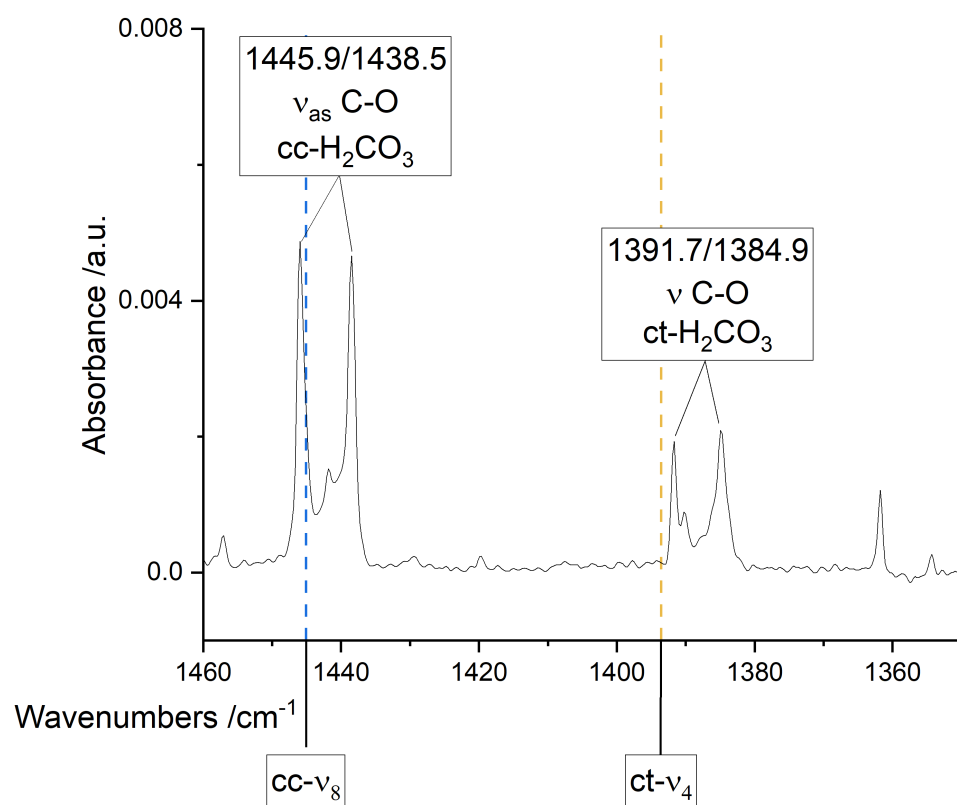


Figure S3: Assignment of the  $\nu$  CO region of the  $\text{H}_2\text{CO}_3$  spectrum. VCI calculated wavenumbers are plotted in dashed lines (blue = cc-conformer; yellow = ct-conformer)

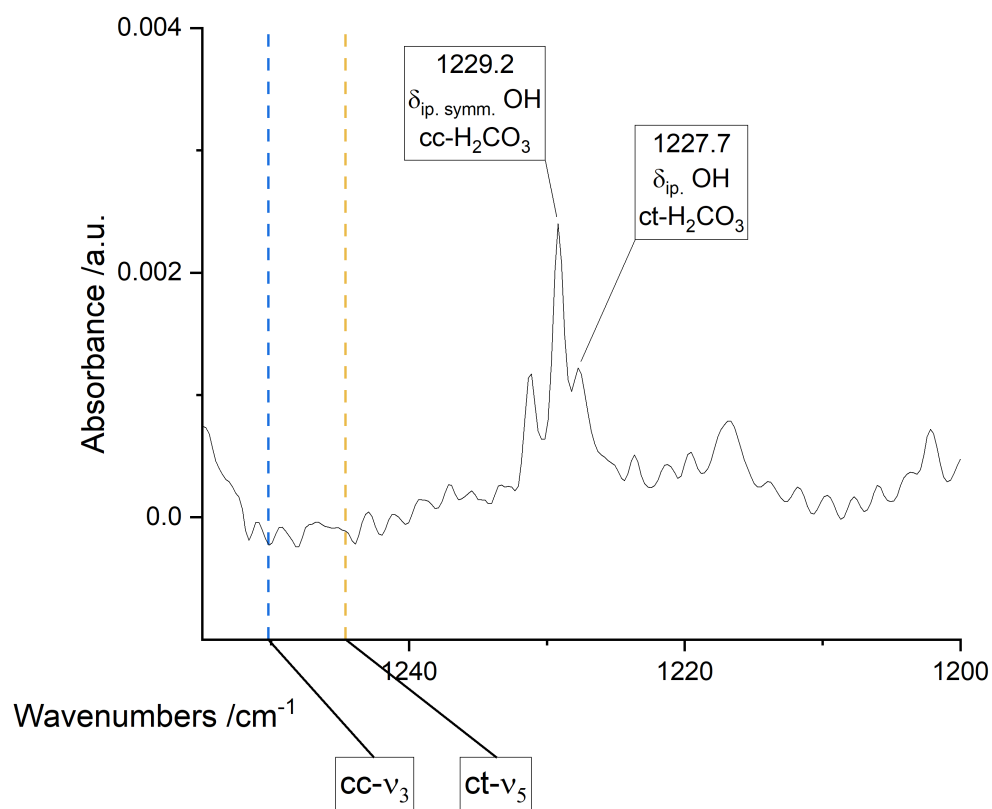


Figure S4: Assignment of the  $\delta_{\text{ip}}$ . OH region of the  $\text{H}_2\text{CO}_3$  spectrum. VCI calculated wavenumbers are plotted in dashed lines (blue = *cc*-conformer; yellow = *ct*-conformer)

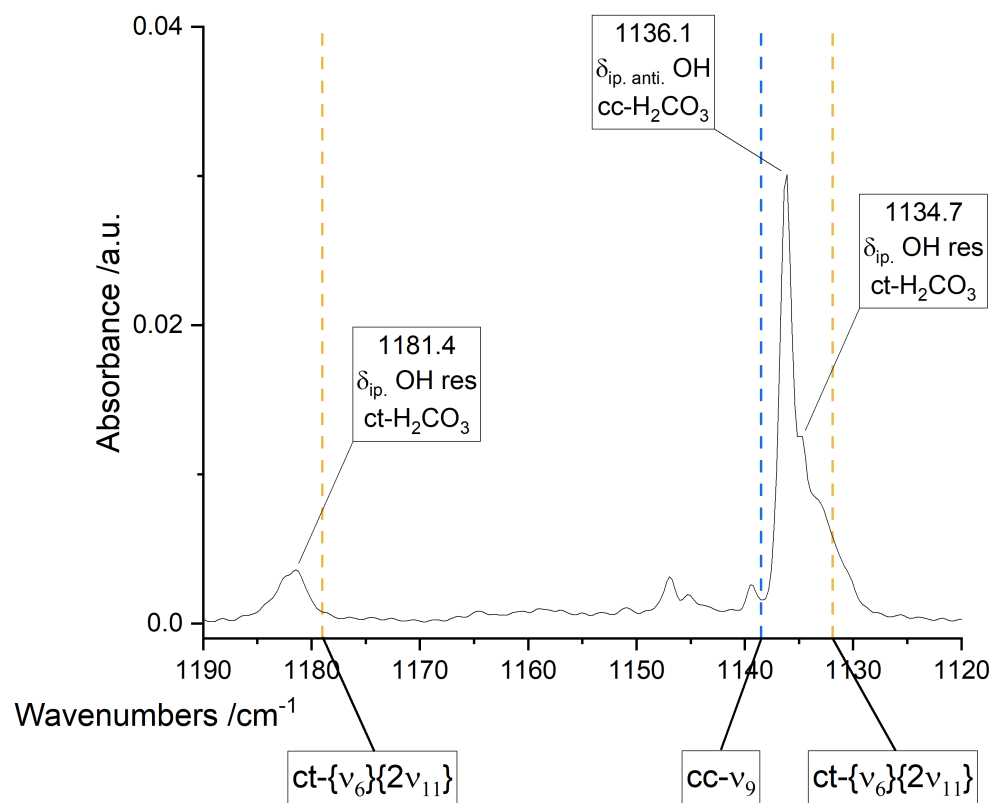


Figure S5: Assignment of the  $\delta_{ip}$ . OH region of the  $H_2CO_3$  spectrum. VCI calculated wavenumbers are plotted in dashed lines (blue = cc-conformer; yellow = ct-conformer)

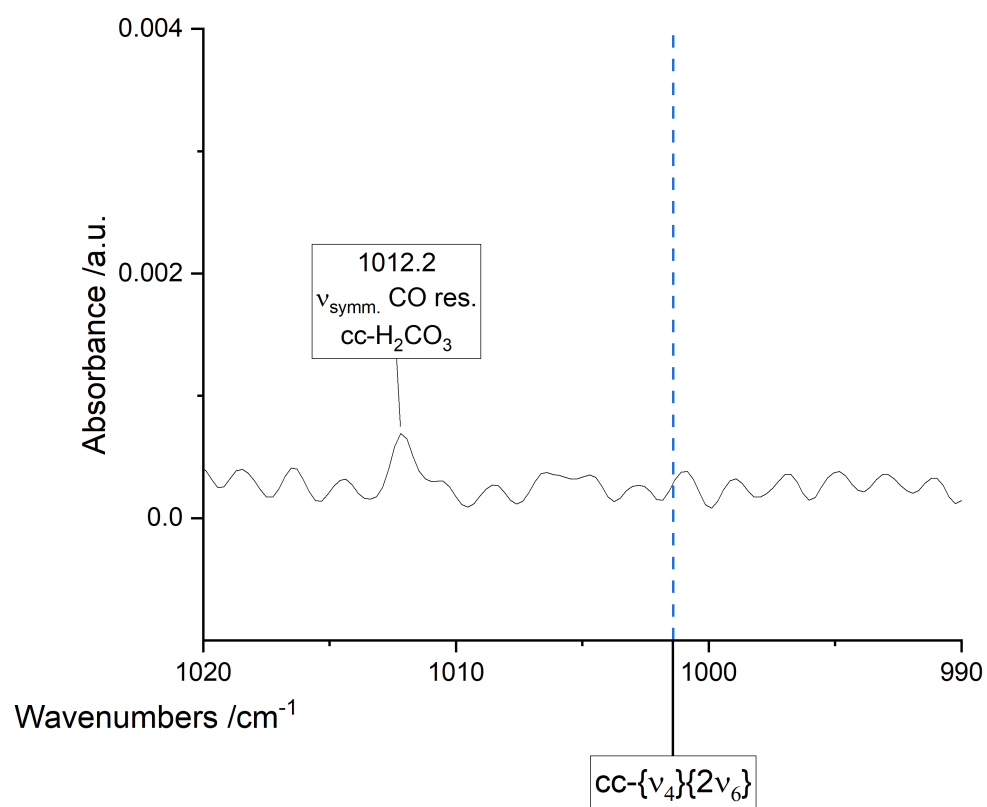


Figure S6: Assignment of the  $\nu_{\text{symm. C-O}}$  region of the H<sub>2</sub>CO<sub>3</sub> spectrum. VCI calculated wavenumbers are plotted in dashed lines (blue = cc-conformer; yellow = ct-conformer)

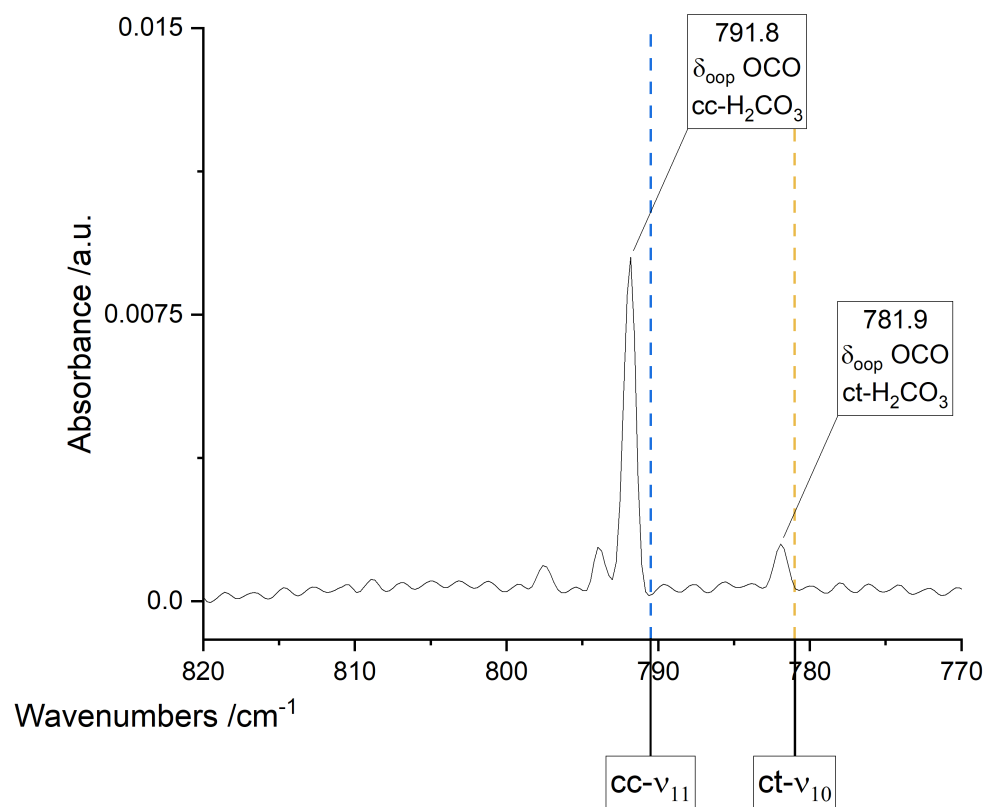


Figure S7: Assignment of the  $\delta_{\text{oop}}$  OCO region of the  $\text{H}_2\text{CO}_3$  spectrum. VCI calculated wavenumbers are plotted in dashed lines (blue = cc-conformer; yellow = ct-conformer)

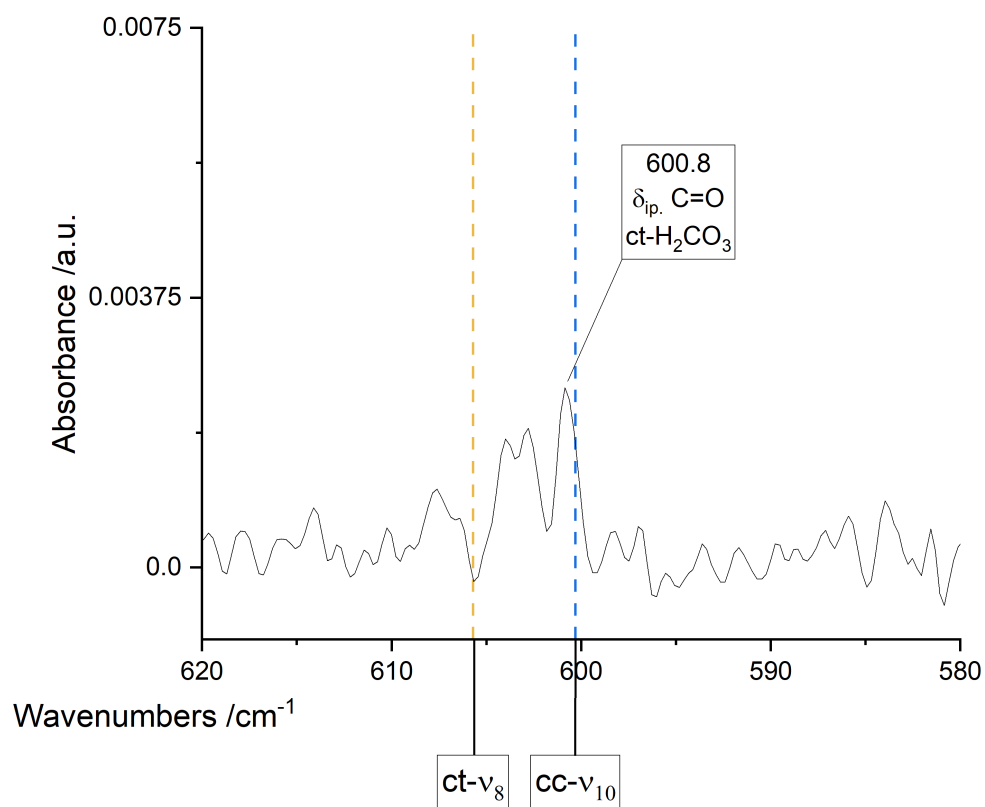


Figure S8: Assignment of the  $\delta_{\text{ip}}$  C=O region of the  $\text{H}_2\text{CO}_3$  spectrum. VCI calculated wavenumbers are plotted in dashed lines (blue = cc-conformer; yellow = ct-conformer)

## The deuterated argon experiment

The assignment of the bands in the deuterated experiment follows the same procedure as the protonated species. In general, there are fewer resonances in the deuterated experiment. The intensities are much lower, which means that no new bands can be assigned for the ct-conformer.

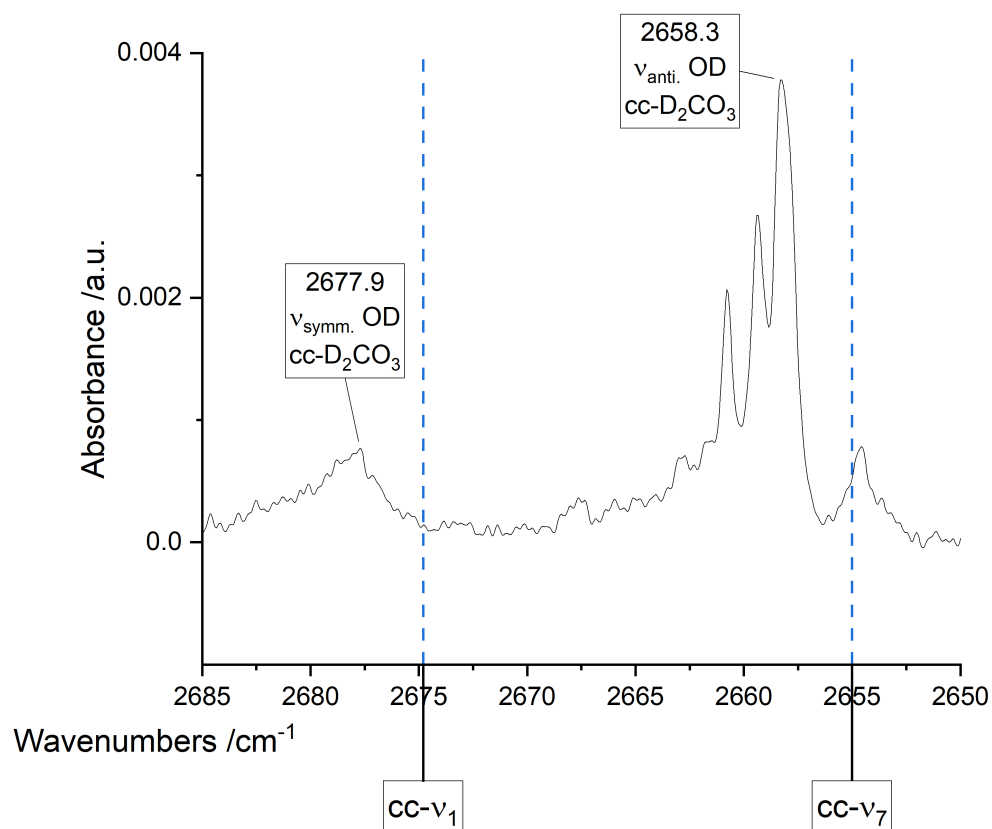


Figure S9: Assignment of the OD stretching region of the  $\text{D}_2\text{CO}_3$  spectrum. VCI calculated wavenumbers are plotted in dashed lines.

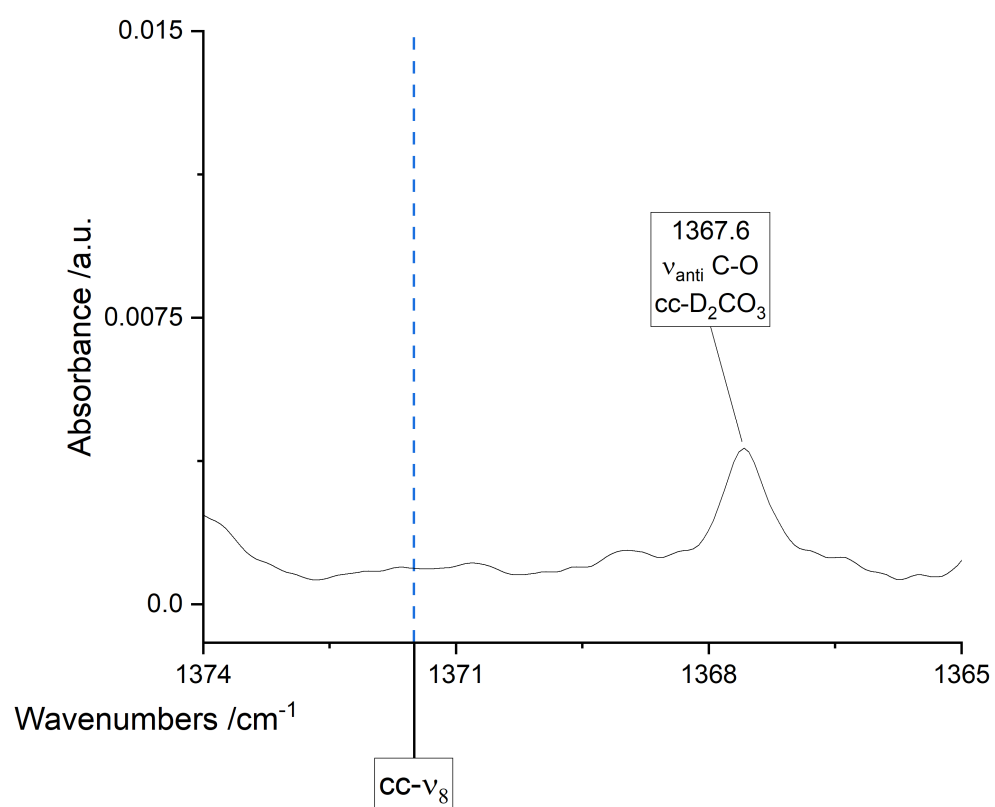


Figure S10: Assignment of the  $\nu_{\text{anti}}$  C-O region of the  $\text{D}_2\text{CO}_3$  spectrum. VCI calculated wavenumbers are plotted in dashed lines.

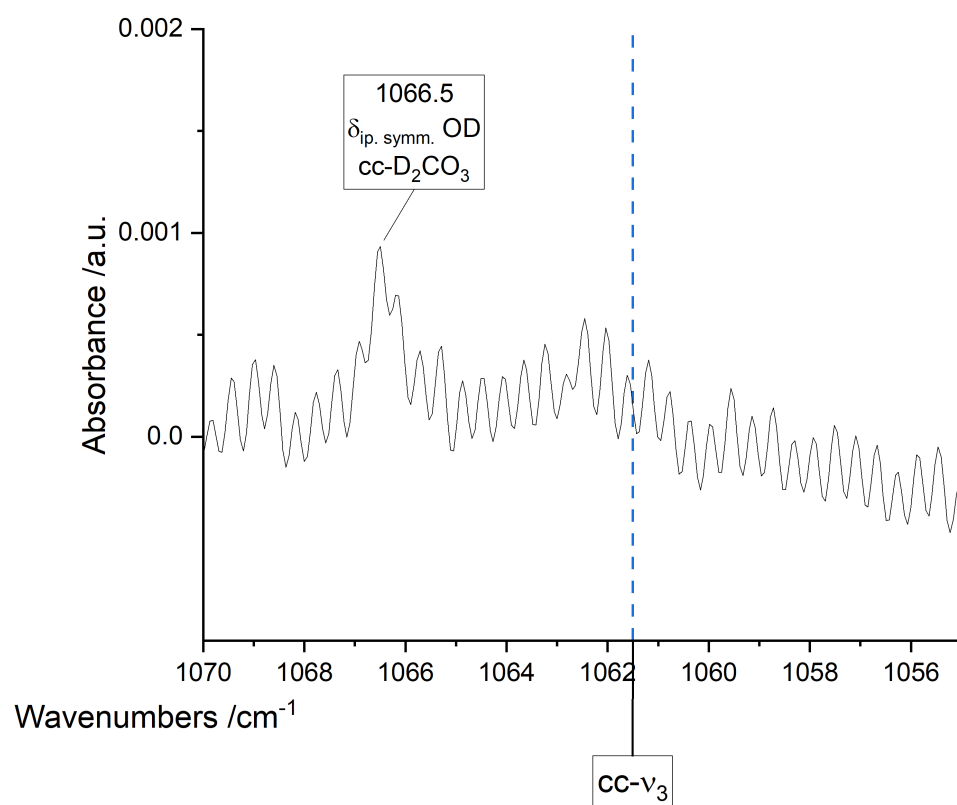


Figure S11: Assignment of the  $\delta_{ip. symm. OD}$  region of the D<sub>2</sub>CO<sub>3</sub> spectrum. VCI calculated wavenumbers are plotted in dashed lines.

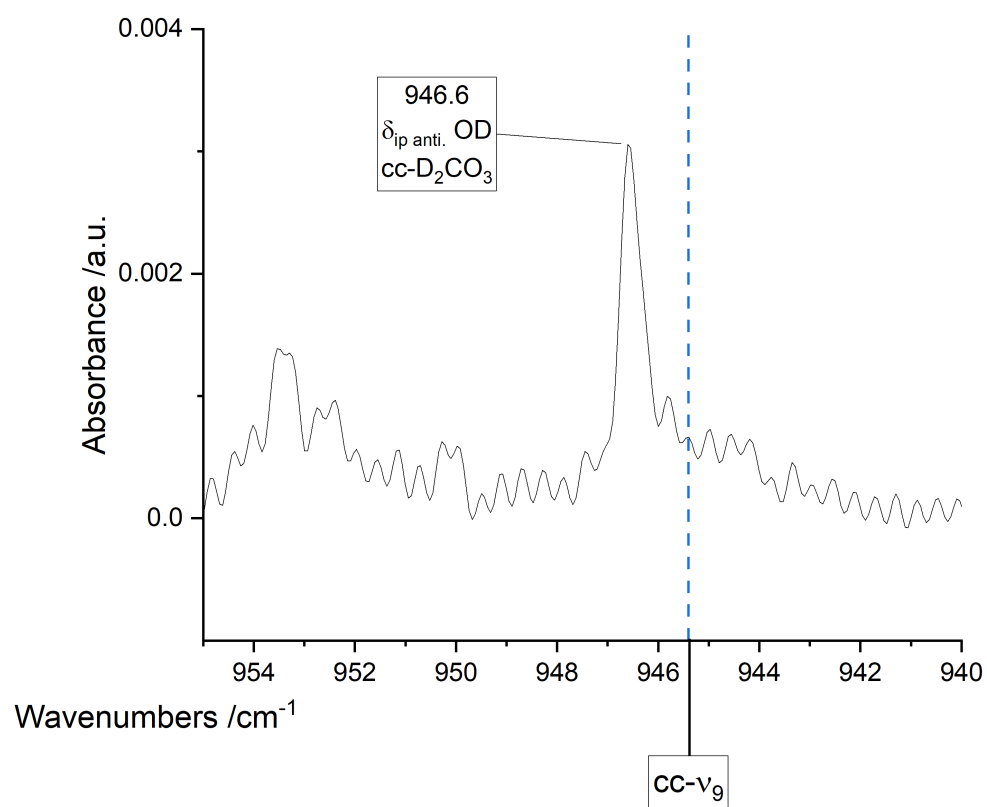


Figure S12: Assignment of the  $\delta_{ip}$ . anti. OD region of the D<sub>2</sub>CO<sub>3</sub> spectrum. VCI calculated wavenumbers are plotted in dashed lines.

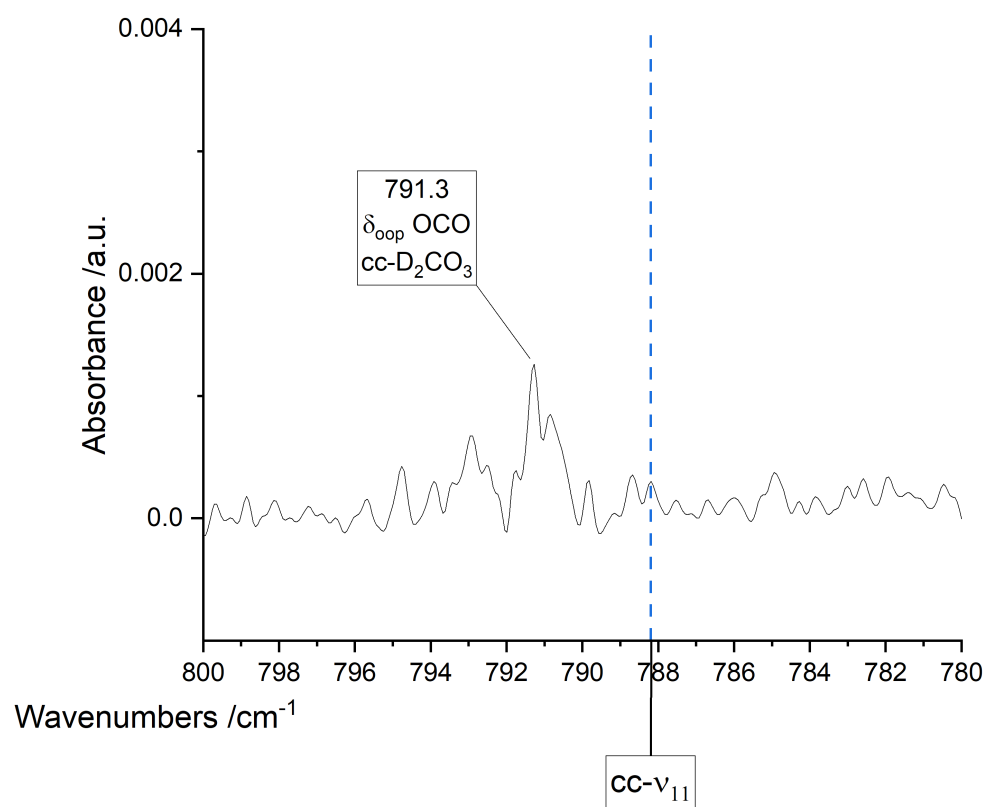


Figure S13: Assignment of the  $\delta_{\text{oop}}$  OCO region of the D<sub>2</sub>CO<sub>3</sub> spectrum. VCI calculated wavenumbers are plotted in dashed lines.

## Visualization of the resonance analysis

In following figures, we visualize the resonance analysis as obtained from the VCI calculation of *cc*-H<sub>2</sub>CO<sub>3</sub> and *ct*-H<sub>2</sub>CO<sub>3</sub> as a so-called *Sankey* plot. This plot represents the resonance analysis as a flow diagram, where the "flow" is a connection between the calculated VCI state energy (on the left-hand side) with its most contributing VCI configurations (on the right-hand side). The thickness of the connecting links visualizes the magnitude of the contributions. For an understanding of the Sankey plot it is also important to know that:

- All contributing fundamentals are colored in blue, all contributing overtones are colored in purple and all contributing combination bands are colored in grey.
- The thickness of the links is taken from the leading coefficients of the calculated VCI configurations. (Alternatively one could take the harmonic overlap value).
- The VCI state energy values are given in cm<sup>-1</sup>.
- The sources on the right show a simplified version of the ket-vector notation of the VCI configuration translated into the spectroscopic notation. E.g., |001010200000) means that the normal modes  $q_3, q_5, 2q_7$  are involved, which translates to  $\nu_8 \nu_7 2\nu_{11}$  in the spectroscopic notation of *cc*-H<sub>2</sub>CO<sub>3</sub> in *C*<sub>2v</sub> symmetry. Note that the labeling of  $\nu$  does not necessarily correspond to their position in the ket-vector because the ket-vector is shown in computational notation (based on normal-modes) and the spectroscopic notation is dependent on the point group of the molecule.

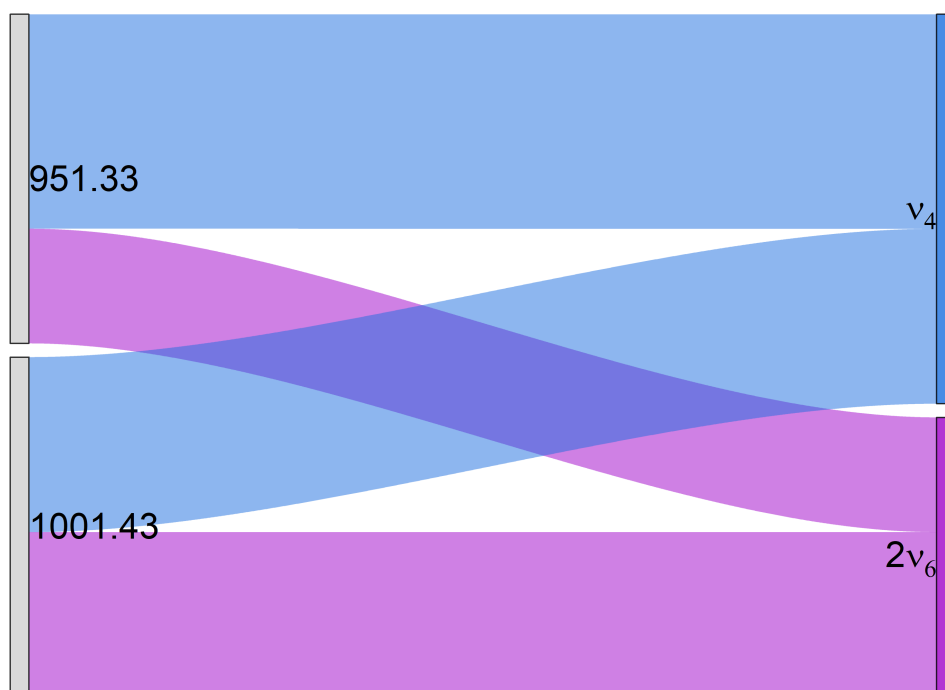


Figure S14: Sankey plot of the VCI analysis for the cc-H<sub>2</sub>CO<sub>3</sub>  $\{\nu_4\}\{2\nu_6\}$  resonance state

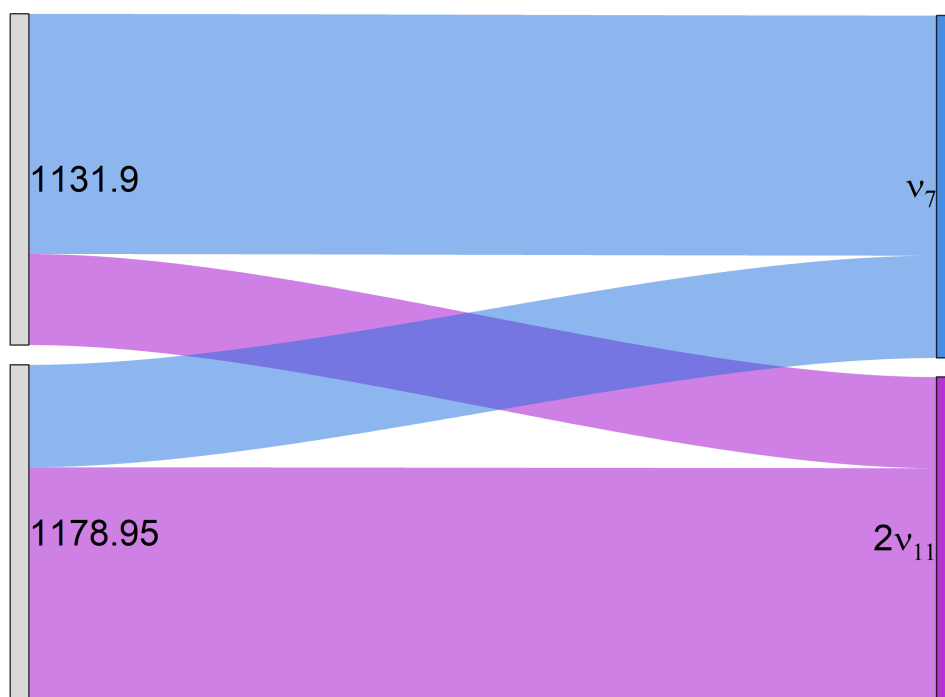


Figure S15: Sankey plot of the VCI analysis for the  $\text{ct-H}_2\text{CO}_3$   $\{\nu_6\}\{2\nu_{11}\}$  resonance state

## References

- [1] K. Oenen, D. F. Dinu, K. R. Liedl, *The Journal of Chemical Physics* **2024**, *160*.
- [2] A. R. Sharma, B. J. Braams, S. Carter, B. C. Shepler, J. M. Bowman, *The Journal of Chemical Physics* **2009**, *130*, 174301.
- [3] J. M. Bowman, T. Carrington, H.-D. Meyer, *Molecular Physics* **2008**, *106*, 2145–2182.
- [4] K. Yagi, C. Oyanagi, T. Taketsugu, K. Hirao, *The Journal of Chemical Physics* **2003**, *118*, 1653–1660.
- [5] C. König, *International Journal of Quantum Chemistry* **2020**, *121*.
- [6] D. F. Dinu, B. Ziegler, M. Podewitz, K. R. Liedl, T. Loerting, H. Grothe, G. Rauhut, *Journal of Molecular Spectroscopy* **2020**, *367*, 111224.
- [7] D. F. Dinu, M. Podewitz, H. Grothe, T. Loerting, K. R. Liedl, *Physical Chemistry Chemical Physics* **2020**, *22*, 17932–17947.
- [8] D. F. Dinu, M. Podewitz, H. Grothe, T. Loerting, K. R. Liedl, *Theoretical Chemistry Accounts* **2020**, *139*.
- [9] D. F. Dinu, M. Podewitz, H. Grothe, K. R. Liedl, T. Loerting, *The Journal of Physical Chemistry A* **2019**, *123*, 8234–8242.
- [10] J. Bernard, PhD thesis, Department of physical chemistry, University of Innsbruck, **2014**.
- [11] A. Engdahl, B. Nelander, *Journal of Molecular Structure* **1989**, *193*, 101–109.
- [12] T. Loerting, C. Tautermann, R. T. Kroemer, I. Kohl, A. Hallbrucker, E. Mayer, K. R. Liedl, *Angewandte Chemie International Edition* **2000**, *39*, 891–894.
- [13] J. Bernard, R. G. Huber, K. R. Liedl, H. Grothe, T. Loerting, *Journal of the American Chemical Society* **2013**, *135*, 7732–7737.